



- 1 Extreme drought-accelerated dissolved carbon metabolism triggers pulsed CO<sub>2</sub>
- 2 outgassing in karst lakes
- 3 Maofei Ni<sup>1</sup>, Weijun Luo<sup>2</sup>, Junbing Pu<sup>3</sup>, Guangneng Zeng<sup>1\*</sup>, Jinxiao Long<sup>1</sup>, Jia
- 4 Chen<sup>2</sup>, Jing Zhang<sup>3</sup>, Xiaodan Wang<sup>1</sup>, Zhikang Wang<sup>1</sup>\*\*
- 5 1. College of Eco-Environmental Engineering, Guizhou Minzu University, Guiyang
- 6 550025, China.
- 7 2. State Key Laboratory of Environmental Geochemistry, Institute of Geochemistry,
- 8 Chinese Academy of Sciences, Guiyang, 550081, China
- 9 3. Karst Research Team, Chongqing Key Laboratory of Carbon cycle and Carbon
- 10 regulation of Mountain Ecosystem, School of Geography and Tourism, Chongqing
- 11 Normal University, Chongqing, 401331, China
- 12 \* Corresponding Author:
- 13 Guangneng Zeng
- 14 Guizhou Minzu University (GMU)
- 15 Address: Guizhou Minzu University, Huaxi District, Guiyang City, Guizhou
- 16 Province, P.R.China 550025
- 17 **Email:** augustinezeng@126.com

https://doi.org/10.5194/egusphere-2025-4284 Preprint. Discussion started: 24 November 2025 © Author(s) 2025. CC BY 4.0 License.





- 18 Zhikang Wang
- 19 Guizhou Minzu University (GMU)
- 20 Address: Guizhou Minzu University, Huaxi District, Guiyang City, Guizhou
- 21 Province, P.R.China 550025
- 22 **Email:** wangzhikang@gzmu.edu.cn



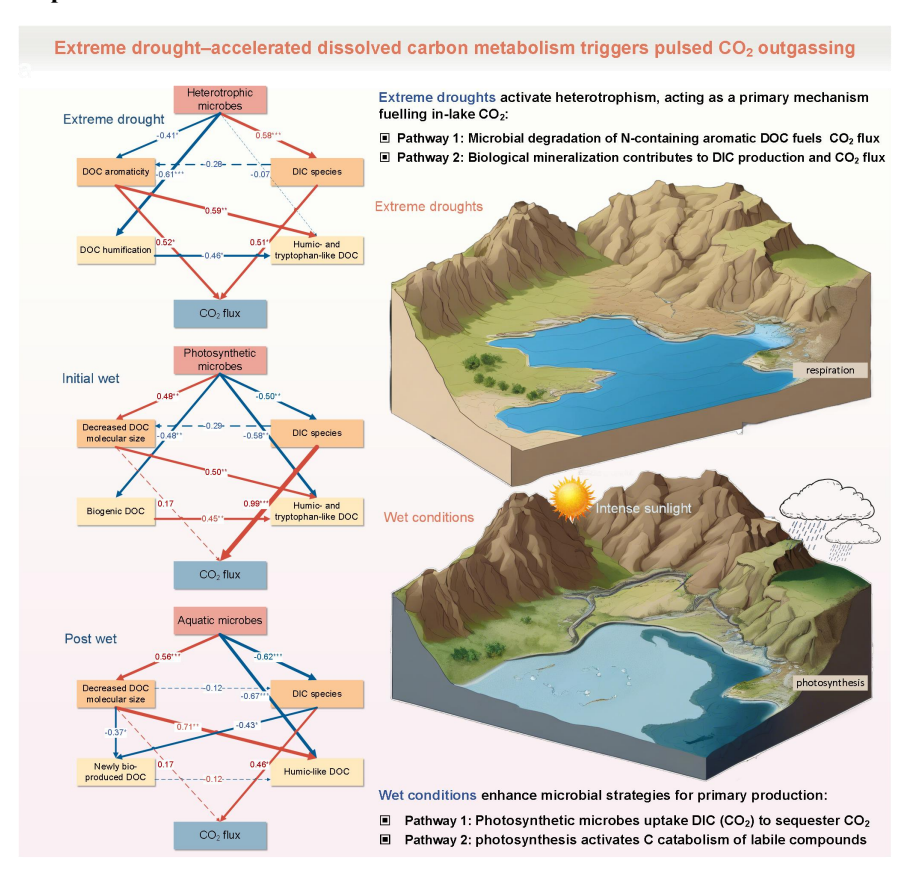


- 23 **Abstract** 24 Karst aquatic ecosystems are important reservoirs of dissolved carbon (C), supporting dynamic CO<sub>2</sub> fluxes through the biological C pump. However, our current 25 understanding of how sophisticated interactions between aquatic microbiomes and 26 27 dissolved C turnover constrain the timing of CO<sub>2</sub> sequestration and emission remains limited. Here we capture an extreme drought event and the ensuing relatively wet 28 29 conditions from systematic investigations in karst lakes, demonstrating that 30 temporally distinct microbiomes are tuned to the metabolic patterns of dissolved C 31 and thereby modulate CO<sub>2</sub> emissions. Specifically, we find that the extreme drought 32 accelerates respiration of dissolved organic C, sharply increasing the CO<sub>2</sub> evasion rate. Wet conditions stimulate photosynthetic uptake of dissolved inorganic C, consuming 33 34 lake CO<sub>2</sub> while promoting labile organic C formation. We therefore propose that pulses of CO<sub>2</sub> emissions from karst lakes occur after wet conditions end, as a 35 consequence of rapid remineralization of newly produced bioavailable organic C, 36 especially during extreme droughts. Our findings highlight the crucial importance of 37 38 managing periodic CO2 outgassing from karst waters under drought conditions for the implementation of region-specific C neutrality strategies. 39 Keywords: Karst waters, aquatic microbiome, dissolved carbon, CO<sub>2</sub> flux, extreme 40
- 41 drought





## 42 Graphical Abstract







# 43 1. Introduction 44 Lakes store, metabolize and release large quantities of natural carbon (C), representing a funnel of aquatic C budget (Bogard et al., 2019; Borges et al., 2022; 45 Evans et al., 2017). Therefore, there is mounting evidence that lakes function as 46 47 "biogeochemical reactors", receiving terrestrial C and continuously cycling the bulk of aquatic C (Pi et al., 2022; Rodríguez-Cardona et al., 2023). Yet to date, the 48 49 mechanisms driving lake C cycling are poorly understood, particularly regarding the 50 underlying factors that constrain C emission (Chen et al., 2022; Mendonça et al., 51 2017). It is estimated that inland lakes, despite covering only ~3% of the land surface, 52 contribute to 38% of aquatic C outgassing (Tranvik et al., 2009). Although the drivers of these emissions are regionally investigated (Maberly et al., 2013; Mu et al., 2023; 53 54 Serikova et al., 2019), a fundamental factor governing C fixation, mineralization, and subsequent uptake or release remains elusive. Deciphering the cycling of dissolved C 55 offers a promising avenue to address this knowledge gap, as it mediates C turnover 56 between organic and inorganic forms and accounts for ~90% of the global C flux from 57 58 terrestrial to aquatic ecosystems (Drake et al., 2020), making it essential for understanding aquatic C budget (Raymond and Hamilton, 2018; Song et al., 2018). 59 Evidence suggests that seasonal wetness and drought control the dynamics of 60 dissolved inorganic C (DIC) concentrations and species (Rehn et al., 2023; Tye et al., 61 2022). These events also alter water-land connectivity and thus the export of dissolved 62 organic C (DOC) to inland waters (Li et al., 2022a; Wang et al., 2024; Yuan et al.,

karst lakes.





2024). Subsequently, aquatic photosynthesis utilizes DIC, while heterotrophic 64 respiration of DOC generates CO<sub>2</sub> (Guo et al., 2023; Leles and Levine, 2023). 65 Consequently, dissolved C turnover and CO<sub>2</sub> emissions are anticipated to be highly 66 interconnected through hydrological and biological mechanisms (Hu et al., 2022; 67 68 Kellerman et al., 2014; Monteith et al., 2023). For example, experimental data suggest that droughts can stimulate dissolved C cycling by transiently accelerating primary 69 70 production and, more persistently, DOC respiration (Harjung et al., 2019). 71 These pervasive turnover and emission of aquatic C, in particular, can be substantial in karst waters. The prevailing view suggests the regional specificity of 72 karst regions, specifically with respect to ecological fragility and the significant role 73 74 in carbonate C sink (Chen et al., 2023; D'Ettorre et al., 2024). Yet, recent reports also highlight significant dissolved C cycling and CO<sub>2</sub> sequestration in karst aquatic 75 ecosystems, attributed to the "biological C pump" effect (He et al., 2024; Sun et al., 76 2022; Zhang et al., 2024). Carbonate weathering can couple with photosynthetic 77 78 uptake of DIC, resulting in self-amplifying CO2 sink during karst water cycle (Liu et 79 al., 2018; Wang et al., 2022). Nevertheless, primary production may trigger DOC catabolism and rapid cycle of active C (Ni et al., 2023; Ni et al., 2022). These critical 80 processes are associated with aquatic biology, but little is known about how lake 81 microorganisms drive dissolved C turnover and ultimately modulate CO<sub>2</sub> emissions in 82





84 Theoretically, microbiome is anticipated to govern internal cycling between DIC and DOC, and this process, in turn, may affect specific CO<sub>2</sub> pathways (Li et al., 2022b; 85 Shangguan et al., 2024). Prior studies found significant DIC uptake by C-fixing 86 microorganisms (Li et al., 2024) and recalcitrant DOC sequestration via heterotrophic 87 88 bacteria in karst aquatic systems (He et al., 2022b; Xu et al., 2023), which potentially regulate CO<sub>2</sub> fixation and outgassing in response to specific pathways of C 89 90 metabolism. Therefore, we hypothesized that microorganisms will interact with 91 dissolved C to establish distinctive CO<sub>2</sub> drivers in karst lakes. To test this hypothesis, 92 we conducted a two-year investigation, capturing an extreme drought event and its 93 following rainfalls, with the aims of revealing: 1) temporal interactions of aquatic microbiome with dissolved C dynamics; 2) specific pathways governing karst lake 94 95 CO<sub>2</sub> flux; and 3) microbially-driven dissolved C turnover and the resulting CO<sub>2</sub> emission or sequestration. Achieving these aims is expected to uncover the underlying 96 mechanisms of C source-sink transformation in karst water environments, ultimately 97 supporting efforts toward C neutrality. 98

## 2. Materials and methods

### 2.1. Study area

99

100

Observations were performed in the karst lakes Hongfeng (HFH), Laoma (LMH) and Baihua (BBH), located between 25°57′ to 26°42′N in latitude and 105°58′ to 106°34′E in longitude (Fig. 1). The catchment geology is predominantly karst lithology i.e., dolomite and limestone. Lake HFH and BHH, two of the largest artificial lakes in

108

109

111

115





105 Guizhou Province, cover surface areas of 57.2 and 14.5 km<sup>2</sup>, with water volumes of  $6.01 \times 10^8$  and  $1.91 \times 10^8$  m<sup>3</sup>, respectively. As a segment of the Maotiao River, the 106 LMH is supplied by several tributaries that connect Lake HFH to BHH. These karst waters are situated in a subtropical monsoon climate zone, with annual temperatures ranging from -7.8°C to 37.5°C. The wet season lasts from May to October, delivering an average annual precipitation of 1130 mm. Specifically, an extreme drought event 110 occurred in 2022–2023, with monthly rainfall <10 mm during the drought (early winter), >100 mm during the initial-wet (early summer), and 50–100 mm during the 112 113 post-wet (autumn) periods. These lakes acting as drinking water sources, are disrupted 114 by agriculture and domestic sewage.

### 2.2. Fieldwork and laboratory analysis

During May to November from 2022 to 2023, our sampling captured an extreme 116 drought event, allowing us to clearly identify the specific temporal scales during the 117 drought, initial-wet and post-wet periods. Spatially, fieldworks were designed to 118 119 incorporate full spectrum of the karst lakes from 32 sampling locations (Fig. 1a). Therefore, a total of 96 water samples were collected from our investigations. In 120 details, we collected surface waters at a depth of ~10 cm and filtered them within 6 121 hours. Filtrates were stored in 1000-mL high-density polyethylene (HDPE) containers 122 123 designed to eliminate headspace and air bubbles. Water samples were filtered using 124 glass microfiber filters (Whatman, GF/F 47 mm, 0.7-µm) for dissolved C measurement, and polycarbonate membrane filters (Millipore, GF/F 47 mm, 0.22-μm) 125

143

144

145





for microbial determination. Samples were refrigerated at 4°C during transport and stored at -70°C for microbiological analysis.

Water temperature and pH were in-situ determined with a portable pH meter 128 129 (PHB-4, Shanghai). Wind velocity was measured using a Testo 410-1 anemometer (Testo, Germany). Total alkalinity was titrated with Alkalinity Test MColortestTM 130 131 (Merck, Germany). DOC concentration was detected using varioTOC cube/select 132 (Elementar, Germany). Chromophoric DOC was determined using a double-beam 133 scanning spectrophotometer (UV-5500PC, Shanghai) with UV-visible absorption 134 spectra ranging from 200 to 700 nm (1-nm interval). Fluorescence DOC was analysed using a RF-6000 Spectrophotometer (Shimadzu, Japan), with excitation and emission 135 136 wavelengths of 200–450 (5-nm interval) nm and 250–600 nm (1-nm interval), respectively. Molecular DOC was characterized using Fourier transform ion cyclotron 137 resonance mass spectrometry (FT-ICR MS). We combined equal volumes of water 138 samples from each lake site, leaving us three composite samples for FT-ICR MS 139 140 analysis. Details on sample pretreatment (solid-phase extraction, SPE) for FT-ICR MS are available in Supplementary Text S1. 141

Genomic DNA in sampling waters was extracted using E.Z.N.A. Water DNA Kit (OMEGA, USA) according to the manufacturers' instructions, and detected with 1% agarose gel electrophoresis. It employed universal primers 341F (5'-CCTAYGGGRBGCASCAG-3') and 806R

161

162

163

164





146 (5'-GGACTACNNGGGTATCTAAT-3') for amplifying the V3–V4 hypervariable
147 region of 16S rRNA, with a GeneAmp PCR System 9700 (ABI GeneAmp, USA). The
148 PCR products were extracted by 2% agarose gel electrophoresis, and recovered from
149 AXYPREP DNA Gel Recovery Kit (Axygen Biosciences, USA) with Tris-HCl for
150 elution. Purified amplicons were pooled in equimolar and sequenced using paired-end
151 on an Illumina MiSeq PE300 (Illumina, USA) following standard protocols.

## 2.3. Data processing and calculation

In this study, we employed a carbonate equilibria-based method for estimating
aqueous DIC, using combinations of water chemistry parameters (pH, water
temperature and total alkalinity) through CO<sub>2</sub>SYS program (Xu et al., 2017). This
program outputs concentrations of DIC species i.e., total DIC, HCO<sub>3</sub>-, CO<sub>3</sub><sup>2</sup>- and
dissolved CO<sub>2</sub>, as well as aqueous partial pressure of CO<sub>2</sub> (pCO<sub>2</sub>), a crucial indication
for potential CO<sub>2</sub> emissions from aquatic environments. The following thin boundary
layer model was used to calculate areal CO<sub>2</sub> flux (mmol m<sup>-2</sup> d<sup>-1</sup>) from the karst waters.

160 Areal 
$$CO_2$$
 flux =  $(pCO_{2water} - pCO_{2ir}) \times k \times K_h$  (1)

This model proposes that the difference between aqueous ( $pCO_{2water}$ ,  $\mu$ atm) and atmospheric  $pCO_2$  ( $pCO_{2air}$ ,  $\mu$ atm) can characterize the impetus and direction for  $CO_2$  transfer. Temporal shifts in *in-situ* atmospheric  $CO_2$  levels (dimensionally convertible to  $pCO_{2air}$ ) are available in Fig. S1. By contrast, gas transfer velocity (k, m d<sup>-1</sup>) can





165 constrain the velocity of water-air CO<sub>2</sub> exchange, which is calibrated from normalized gas transfer velocity ( $k_{600}$ , cm h<sup>-1</sup>) using water temperature and Schmidt number. 166 Specifically, k or  $k_{600}$  serves as a function of water turbulence, empirically modelled 167 by wind velocity in lakes and lentic rivers. Henry's constant (*K*<sub>h</sub>, mmol m<sup>-3</sup> μatm<sup>-1</sup>) 168 169 calibrated from in-situ temperature and pressure, characterizes CO2 equilibrium at water-air interfaces. Details for chemical calculations of DIC species and thin 170 171 boundary layer model see Supplementary Text S2. 172 We analysed UV-visible and fluorescent spectroscopy for understanding DOC 173 component, origin and fate. Specifically, DOC-normalized absorption coefficient SUVA<sub>254</sub> (L mg<sup>-1</sup> m<sup>-1</sup>), an indicator of DOC aromaticity, was computed as the 174 175 absorption coefficient (a<sub>254</sub>, m<sup>-1</sup>) divided by DOC concentration (mg L<sup>-1</sup>). Spectral slope S<sub>275-295</sub>, a proxy for DOC relative molecular weight, was calculated by 176 177 nonlinearly fitting an exponential function to the absorption spectrum from 275 to 295 nm. Fluorescence index (FI) increases with intensified biological activity, and 178 179 indicates allochthonous (< 1.4) and autochthonous (> 1.9) inputs for aquatic DOC, which was calculated as the ratio of emission intensity at 470 nm to 520 nm with an 180 excitation of 370 nm. Biological index (BIX), a proxy for freshness of biologically 181 produced DOC, was calculated as the ratio of emission intensity at 380 nm to 430 nm, 182 183 using an excitation of 310 nm. Humification index (HIX), characterizing to DOC humification and biodegradability, was expressed as the ratio of total emission 184

intensities at 435-480 nm divided by 300-345 nm, at an excitation of 254 nm. Parallel





factor analysis (PARAFAC) was used to identify primary DOC component by
separating excitation-emission matrices into independent fluorophores. The
PARAFAC modelling employed residual and split-half analyses for component
selection and correspondence validation.

190 FT-ICR MS analysis was conducted to examine dissolved organic matter (DOM, 191 represents the specific material form of the general DOC) composition using a 192 molecular formula calculator based on criteria with elemental combinations of  $C_{0\text{--}\infty}H_{0\text{--}\infty}O_{0\text{--}\infty}N_{0\text{--}1}S_{0\text{--}1}. \text{ Peaks were detected within S/N} > 4 \text{ and a mass accuracy of } \leq \pm 1$ 193 194 ppm. Van Krevelen diagrams plotting H/C against O/C were employed to visualize 195 FT-ICR MS data. Seven DOM compositions were extracted based on the elemental 196 ratios of H/C and O/C (Ni et al., 2024), involving carbohydrates, amino-sugars, saturated compounds, tannins, lignin, unsaturated hydrocarbons and condensed 197 aromatic structures. The elements (C, H, O, N, P and S), and formulas (CHO, CHOS, 198 199 CHON, CHOP, CHONS, CHONP, CHOSP and CHONSP) were identified based on 200 molecular exact mass and matched against a molecular formulas database (Yan et al., 201 2024). The modified aromaticity index (AI-mod) and nominal oxidation state of carbon (NOSC) were calculated as follows: 202

$$AI\_mod = \frac{1 + C - \frac{1}{2}O - S - \frac{1}{2}(N + H)}{C - \frac{1}{2}O - N - S}$$
 (2)

$$NOSC = \frac{4C + H - 3N - 20 - 2S}{C}$$
 (3)





Alpha diversity, calculated using Mothur (<a href="https://mothur.org/wiki/calculators/">https://mothur.org/wiki/calculators/</a>), was used to assess microbial community through the indices Coverage (community coverage), Chao (community richness) and Shannon (community diversity). We analysed microbial community and its relative abundance, ranking the top 20 microorganisms at genus level. Using Tax4Fun, we converted 16S into prokaryotic classification profiles in the KEGG database, enabling KEGG functional annotation for 16S RNA gene sequences. It provides insights into potential microbial functions based on their composition and abundance in aquatic environments, and specifically presents information on KEGG Orthology in this study.

### 2.4. Quality control

Water collection and analysis followed the standard procedures, as proposed by the American Public Health Association (1985). The pH probe was calibrated with 6.86 and 9.18 pH standard solution at 25°C, ensuring ±0.01 pH unit accuracy. Water temperature and wind velocity were accurate to ±0.5°C and ± (0.2 m/s + 2% of measurements), respectively. Alkalinity Test MColortestTM measured total alkalinity with < 3% uncertainty. DIC species calculated from water chemistry may be overestimated due to non-carbonate alkalinity (Liu et al., 2020). We specifically assessed that non-carbonate alkalinity from nitrogen, phosphorus and organic C can result in a maximum 29.5% overestimation of DIC species. Consequently, we corrected this overestimation by using measured DIC concentrations (Fig. S2), which





223 converted systematic errors into instrument errors (< 2%) for all DIC datasets. UV measurements were 10% replicated, suggesting an uncertainty of < 2 %. The inner 224 225 filter effect of fluorescence data can be neglected since absorbances at 254 nm were all below 0.3 (Ohno, 2002). Excitation-emission matrices were corrected for Raman 226 227 and Rayleigh scatterings through interpolation, and fluorescence intensity (A.U.) was normalized to Raman Unit (R.U.) via water Raman peak areas (Ni et al., 2024). 228 229 FT-ICR MS and microbial analysis were conducted by China National Analytical 230 Centre (Guangzhou, China) and Majorbio Bio-Pharm Technology Co. Ltd. (Shanghai, 231 China), respectively. 232 2.5. Statistical analysis 233 Normality and homogeneity of variance were assessed using Kolmogorov-Smirnov test and Levene's test, respectively. Variables were log-transformed as needed to 234 ensure normality assumptions. One-way analysis of variance (ANOVA) with Tukey 235 HSD post hoc was employed to evaluate statistical differences across DIC species, 236 237 DOC compositions and microbial variables. Correlation analysis was used to assess possible associations within or between dissolved C, CO2 flux and microbial variables. 238 We introduced a structural equation model (SEM) to examine how aquatic 239 microorganisms interact with dissolved C and ultimately influence CO2 flux through 240 241 both direct and indirect pathways. We initially excluded the variables with nonlinear relationships (e.g., alpha diversity and Tax4Fun) to derive comparable standardized 242 path coefficients. We further established and specified 6 latent variables according to 243

260

261

262

263

264





245 the SEM, we hypothesized that 1) photosynthetic and heterotrophic microbes will preferentially associate with DIC for anabolism and DOC for catabolism, respectively; 246 and 2) dissolved C dynamics and CO2 flux are intertwined due to carbonate chemistry, 247 248 biogenic, and terrestrial regulations. The SEM with partial least squares path modelling was performed using the plspm package in R (Version 4.1.3). Statistical 249 250 analyses and figures preparing were conducted using and OriginPro 2024 and 251 MATLAB 2018. 252 3. Results 3.1. DIC species and CO<sub>2</sub> emissions 253 254 The significant carbonate kinetics in karst waters present an opportunity to understand the dynamics of aqueous DIC species. This study captured strong seasonality in water 255 chemistry (Table 1), particularly with lower pH and water temperature during the 256 extreme-drought period (p < 0.001 by ANOVA). *In-situ* measured total alkalinity 257 (range: 2178.7-6210.8 μeq L<sup>-1</sup>), along with DIC (range: 1538.7-6206.0 μmol L<sup>-1</sup>) and 258 HCO<sub>3</sub>- (range: 918.4–5970.6 μmol L<sup>-1</sup>), had no temporal variations across the periods 259

the loadings of their associated observed variables (see Supplementary Text S3). In

(p > 0.05). Extreme drought caused lower aqueous  $CO_3^{2-}$  but higher dissolved  $CO_2$ 

corrected concentrations of DIC species by eliminating systematic errors from

HCO<sub>3</sub>-, and 38.7% for dissolved CO<sub>2</sub> (Fig. S2).

non-carbonate alkalinity, reducing average uncertainties of 6.8% for DIC, 7.0% for

levels in comparison to wet conditions (p < 0.001, Fig. S3). It should be noted that we





265	To estimate potential CO <sub>2</sub> emissions from the study lakes, we calculated aqueous
266	$pCO_2$ , $k$ and areal $CO_2$ flux (Fig. 1). These lakes had a broad range of aqueous $pCO_2$
267	levels, spanning from 20 to 13479 µatm across sampling locations (Fig. 1b). We found
268	that extreme drought (4437 $\pm$ 3468 $\mu atm)$ unexpectedly caused a $\sim\!\!$ five-fold increase
269	in mean $p$ CO <sub>2</sub> relative to initial- (804 $\pm$ 1080 $\mu$ atm) and post-wet periods (928 $\pm$ 1728
270	μatm, p < 0.001), which can escalate to ~ten-fold when considering median $p$ CO <sub>2</sub> (Fig.
271	1b). Indeed, our dataset reveals that 61% of samples were oversaturated with CO <sub>2</sub>
272	relative to atmospheric equilibrium (Fig. S1), attributable to high pCO <sub>2</sub> levels during
273	extreme droughts. Gas transfer velocity $k$ showed no significant temporal shifts (p >
274	0.05), ranging from 0.37–2.28 m $d^\text{-1}$ with a mean of 0.62 $\pm$ 0.26 m $d^\text{-1}$ (Fig. 1c). This is
275	slightly lower than previously reported global average of 0.74 m d <sup>-1</sup> from a similar
276	empirical model based on wind speed (Raymond et al., 2013). We estimated areal $CO_2$
277	flux to be 42 $\pm$ 79 mmol $m^{2}$ d $^{1}$ (range: -24–459 mmol $m^{2}$ d $^{1}$ ) from the karst lakes.
278	However, it is also noted that the bulk of samples during wet periods were
279	undersaturated (Fig. 1d). We show that extreme drought increased areal CO <sub>2</sub> efflux
280	sharply (111 $\pm$ 104 mmol m $^{\text{-}2}$ d $^{\text{-}1}$ ), relative to initial- (6 $\pm$ 22 mmol m $^{\text{-}2}$ d $^{\text{-}1}$ ) and
281	post-wet periods (10 $\pm$ 26 mmol $m^{2}$ d^{1}) (p < 0.001). Our findings, therefore, may
282	partially deviate from the previous understanding of aquatic karst carbon sinks (An et
283	al., 2015; Binet et al., 2020; Liu et al., 2010), indicating that karst lakes could be a
284	significant source of CO <sub>2</sub> driven by extreme drought events.





# 285 3.2. DOC composition, origin and fate We used spectroscopic and molecular methods to assess DOC composition, origin and 286 fate (Fig. 2 and 3). Aqueous DOC concentrations had a ~30-fold variation (range: 287 0.76–22.1 mg L<sup>-1</sup>) across the samplings (Fig. 2a). Extreme drought apparently 288 289 elevated DOC concentrations to an average of $12.4 \pm 3.7$ mg L<sup>-1</sup>, relative to initial- $(5.4 \pm 2.3 \text{ mg L}^{-1})$ and post-wet periods $(5.7 \pm 1.6 \text{ mg L}^{-1})$ (p < 0.001). DOC 290 291 aromaticity descended significantly across the periods, with initial-wet > post-wet > 292 extreme drought (p < 0.01), as suggested by SUVA<sub>254</sub>. By contrast, relative molecular 293 weight of DOC, indicated by S<sub>275-295</sub>, was higher during extreme-drought period than 294 wet periods (p < 0.05). We were able to identify DOC fluorescent component through PARAFAC, demonstrating two distinct humic-like (C1) and one tryptophan-like DOC 295 296 (C2) across the periods (Fig. 2b). The temporal abundances differed significantly (p < 0.001), with %C1 > %C2 during the extreme drought yet %C1 < %C2 during wet 297 conditions (Fig. S4). These karst waters received both allochthonous and 298 autochthonous inputs, with 80% of samples falling within the FI range of 1.4–1.9 (Fig. 299 300 2c). As suggested by BIX, we found biologically produced young DOC was more abundant during initial-wet than extreme-drought period (p < 0.05). However, DOC 301 humification proxied by HIX was notably greater during the extreme drought than 302 303 that in the wet conditions (p < 0.01). It captured the molecular formulas for a total of 8060, 8636 and 8403 304 FT-ICR-MS compounds in lake LMH, HFH and BHH, respectively (Fig. 3). The 305





307 distributions, as well as exact mass in van Krevelen Diagram (Fig. 3a). The study lakes showed a similar range of DOM exact mass, varying from 114.031694 to 308 1121.181055 Da. We suggest that these lakes were governed by low-molecular-weight 309 310 DOM, with 80%, 74%, and 77% of the detected molecules for LMH, HFH, and BHH having an exact mass < 500 Da, respectively. The summed intensity was highly 311 312 variable for each DOM molecular category, notably with lignin compounds (or carboxy-rich acyclic molecules) comprising 83%-84%, followed by saturated 313 compounds at 11%-13% across lakes. Amino-sugars also represented a notable 1.8%-314 315 2.3%, while carbohydrate, tannins, unsaturated hydrocarbons and condensed aromatic structures each occupied ≤ 1% across all molecular categories. These DOM molecules 316 317 were largely comprised of atomic groups CHO (44.8%–49.2%), CHOS (17.2%– 318 25.5%), CHON (19.2%–26.6%) and CHONS (5.6%–6.3%) (Fig. 3b). Each karst lake 319 shared a comparable average AI<sub>mod</sub> across FT-ICR-MS compounds (p > 0.05), while NOSC was higher in lake BHH (-0.29  $\pm$  0.48) than that in LHM (-0.32  $\pm$  0.48) (p < 320 321 0.01, Fig. 3c). 3.3. Aquatic microbiome in the karst lakes 322 To evaluate microbial processes in the karst lakes, we examined temporal variability 323 of microbiome from 89 samples (Fig. 4). For the microbial diversity, a total of 121– 324 351 ASV (14382 sequences), 236–479 ASV (40251 sequences) and 143-445 ASV 325 (42507 sequences) were assigned during the extreme-drought, initial-wet and post-wet 326

molecular formulas were classified into distinct categories based on H/C and O/C





328 the aquatic environment (Fig. 4a), as indicated by Chao (initial wet > post wet > 329 extreme drought, p < 0.05) and Shannon (initial wet > post wet and extreme drought, p < 0.05). However, microbial coverage was higher in the extreme-drought period (p 330 331 < 0.01). The top 3 microorganisms were Acinetobacter, CL500-29 marine group and 332 Cyanobium PCC-6307 at genus level, with the average relative abundances of 11.6% 333  $\pm 10.3\%$ ,  $10.3\% \pm 5.58\%$  and  $5.68\% \pm 3.91\%$ , respectively (Fig. 4b). Acinetobacter 334 and CL500-29 marine group, important for C catabolism, had increased relative 335 abundance during the extreme drought. By contrast, photosynthetic microorganisms 336 Cyanobium\_PCC-6307 and g\_norank\_f\_norank\_o\_Chloroplast were more abundant during the initial-wet period (Fig. 4b). Therefore, we found that amino acid 337 338 catabolism was significant under extreme droughts, while carbohydrate anabolism was predominant under wet conditions (Fig. 4c, p < 0.001). 339 4. Discussion 340 341 4.1. Temporal interactions of aquatic microbiome with dissolved C dynamics Karst aquatic ecosystems, with rapid kinetics of carbonate chemistry and biological 342 metabolism involved, may develop associated strategies for dissolved C turnover (He 343 et al., 2024; Ni et al., 2023; Xi et al., 2024). Here, our results show the consistent 344 345 shifts of dissolved C with aquatic microbiome in karst lakes. Extreme droughts, for instance, set the stage for substantial proliferation of heterotrophic microbes (Fig. 4b) 346 and thus microbial degradation of enriched DOC (Fig. 2a). As labile DOC is 347

periods, respectively (Fig. S5). Rainfall increased microbial richness and diversity in





DOC. This aligns with recent observations in karst and thermokarst lakes (Hu et al., 349 350 2023; Ni et al., 2022), as also evidenced by the parallel increase in CO<sub>2</sub> levels (Fig. 1b) and decrease in DOC aromaticity (Fig. 2a), suggesting that in-lake aromatic 351 352 compounds are partially labile during extreme droughts. By analysing DOC molecular composition, we specifically found that N-containing, rather than S-containing 353 354 aromatics are more bioavailable for heterotrophic microorganisms (Fig. S6 and 355 Supplement table S1). Rainfall accelerates atmospheric CO<sub>2</sub> uptake and CO<sub>3</sub><sup>2-</sup> generation in karst 356 aquatic environments (Zhao et al., 2024), which, combined with photosynthetic 357 358 uptake of DIC, provides conditions for the enhancement of photosynthetic microorganisms (Fig. 4b). This explains the consistently low CO<sub>2</sub> levels during wet 359 periods (Fig. 1b), aside from the known dilution effect (Ni et al., 2019). Here, we 360 suggest that initial rainfall following extreme droughts substantially boosts microbial 361 362 richness and diversity (Fig. 4a), possibly due to amplified terrestrial inputs and rejuvenated aquatic biology (Fig. S7). Moreover, we were able to examine the 363 associations between DOC molecular compositions and microorganisms, revealing 364 that photosynthetic microorganisms generate substantial quantities of biodegradable 365 366 DOC e.g., carbohydrate and lipid-like compounds (Fig. S6 and Supplement table S1). Therefore, our results indicate season-specific microbial strategies for dissolved C 367 metabolism in karst lakes. 368

exhausted, these microbes are compelled to metabolize typically more refractory





#### 4.2. Specific pathways governing karst lake CO<sub>2</sub> flux

Microbiome-driven dissolved C turnover can further alter CO<sub>2</sub> dynamics, especially in lakes with long-term hydraulic retention and active biological processes (Lindström and Bergström, 2004). Our results show that the photosynthesis-driven associations between microbiome, dissolved C, and CO<sub>2</sub> flux emerged substantially during initial-wet periods (Fig. S8). Studies previously predicted self-amplifying photosynthesis driven by carbonate dissolution in karst waters (He et al., 2022a; Liu et al., 2010). Here, we present direct evidence that photosynthetic microorganisms dominate the microbial communities during the initial-wet period (Fig. 4b). Extreme drought, however, decouples the linkages between dissolved C and CO<sub>2</sub> flux from photosynthetic microorganisms. Respiration of DOC e.g., tryptophan-like component in turn fuels lake CO<sub>2</sub> during the extreme-drought period (Fig. S8). Our data allow us to extrapolate that amino acids, aliphatic compounds and small molecular organic acids serve as primary substrates driving CO<sub>2</sub> production and emissions in these lakes (Fig. 9 and Supplement table S1).

Using SEM, we clearly demonstrate the specific pathways governing lake CO<sub>2</sub> transfer across the periods (Fig. 5). Our observations reinforce that extreme droughts stimulate microbial metabolism of aromatic DOC and contribute to CO<sub>2</sub> outgassing from the study lakes (Fig. 5a). Nevertheless, it emerged an alternative C metabolism pathway during the initial-wet period (Fig. 5a): photosynthetic microorganisms





constrain DIC species and subsequent CO<sub>2</sub> flux in lakes. This photosynthetic pathway persisted during the post-wet period, yet we found a specific pathway involving aquatic microbes that promotes a decrease in molecular size and subsequent increases in humic-like abundance (Fig. 5a). This observation aligns with a previous study in karst aquatic ecosystems (Xia et al., 2022), suggesting that intense photosynthesis produces labile compounds and subsequently activates the catabolism of DOC pool, ultimately resulting in the selective accumulation of recalcitrant compounds. These findings, complement prior evidence from biodegradation assays (Ni et al., 2022), providing a new insight into photosynthetic products triggering significant microbial activities and dissolved C turnover in karst lakes.

## 4.3. Implications for biologically driven C cycling in karst waters

Karst aquatic ecosystems typically represent strong interactions between microbial metabolism and dissolved C turnover, driven by the known "biological C pump" (Yi et al., 2021; Zhang et al., 2024). While the specific C sink from this mechanism is well-documented (Cao et al., 2018; Chen et al., 2023; Sun et al., 2021), the causes of periodic C evasion from karst waters are still questionable. In this study, we propose that extreme droughts yield large CO<sub>2</sub> emissions from the karst lakes, increasing >10 times on average relative to wet conditions (Fig. 1d). Droughts apparently accelerate heterotrophic respiration of DOC, acting as a primary mechanism fuelling in-lake CO<sub>2</sub>. Drought-enriched heterotrophic microorganisms extensively deplete labile DOC, and even resort to metabolizing previously recognized recalcitrant compounds. Aromatic

425

426

427

428

429





to be activated through photochemistry (Hu et al., 2023). Here, our results 411 demonstrate a clear mechanism by which microbial degradation of N-containing 412 aromatic compounds contributes to C metabolism (Fig. S6), indicating that extreme 413 414 droughts suppress biological C sink in karst lakes. 415 Wet conditions in karst lakes, in contrast, show a distinct pathway governed by 416 aquatic photosynthesis (Fig. 5b), aligning with the prior theory regarding karst 417 biological C sink (Liu et al., 2018). This stimulates a substantial uptake of CO2 and 418 thus limit lake C emission. Our observations provide direct evidence that photosynthetic microorganisms produce carbohydrates and promote the formation of 419 420 lipid-like (Fig. S6) as well as other low-molecular-weight compounds (Fig. S8). These labile DOC quickly engage in subsequent biological processes, accelerating the 421 422 proliferation of heterotrophic microorganisms. Our efforts to upscale this mechanism demonstrate a clear causality: 1) catabolism of photosynthetically derived labile DOC 423 424 stimulates heterotrophic microorganism growth; 2) recalcitrant DOC accumulates

DOC, for instance, characterized by microbial resistance, has recently been reported

relatively as heterotrophic respiration increases, even though aromatic compounds are

partially utilized; 3) a priming effect is triggered, promoting both labile DOC

mineralization to CO<sub>2</sub> and the sequestration of recalcitrant DOC. These findings

highlight that biologically driven organic C turnover critically determine the CO<sub>2</sub>

uptake or release in karst aquatic ecosystems.





Overall, as we initially hypothesized, aquatic microbiome interacts with dissolved C dynamics, establishing the distinctive CO<sub>2</sub> driving mechanisms that particularly fluctuate with biochemical timing in karst lakes. It is anticipated that pulses of CO<sub>2</sub> emissions will occur after wet conditions end, particularly under drought conditions, as a result of rapid decay of photosynthetically derived organic C. Therefore, managing C sink in karst aquatic systems depends heavily on mitigating the sudden bursts of DOC respiration, especially the dramatic increased CO<sub>2</sub> release during extreme droughts. Our results indicate that wet conditions significantly enhance biological strategies for CO<sub>2</sub> uptake in karst aquatic ecosystems, highlighting the crucial role of mitigating climate change-induced droughts in strengthening karst C sink.

#### 4. Conclusion

Karst lakes represent distinctive microbial pathways for dissolved C metabolism and subsequent CO<sub>2</sub> sequestration or emission. Here, we specifically reveal the temporal dynamics of CO<sub>2</sub> fluxes driven by periodic interactions between aquatic microbiome and dissolved C turnover in the study karst lakes. We show that extreme droughts accelerate the proliferation of heterotrophic microbes and thus rapid respiration of DOC, resulting in a sharp increase in CO<sub>2</sub> emissions. By contrast, wet conditions stimulate aquatic photosynthesis, which consumes DIC and sequesters CO<sub>2</sub> within the lakes. We highlight that exhausted DOC compels heterotrophic microorganisms to metabolize refractory N-containing aromatic compounds, while photosynthetic





451 microorganisms promote the formation of labile DOC compounds. These specific microbial strategies indicate that pulsed CO2 outgassing from karst lakes occurs after 452 periods of high photosynthetic activity, with the magnitude being significantly 453 amplified during extreme droughts. Therefore, we propose that managing periodic 454 455 CO<sub>2</sub> outgassing, particularly during droughts, is essential for developing C neutrality 456 in karst waters. Code/Data availability 457 458 The full dataset used for the evaluation of this study is publicly available at 459 https://figshare.com/s/7475752c5f7b19718199. 460 **Declaration of Competing Interest** All authors agree this submission and the authors declare that there is no conflict of 461 interests regarding the publication of this article 462 463 **Author contributions** The project was conceived by M.N. and Z.K. M.N. directed and managed the study, 464 as well as prepared the first draft of the manuscript. Z.K. collected and analysed 465 samples, contributed to data interpretation and paper writing. G.Z. specified the 466 experimental conditions and measured CO<sub>2</sub> data. W.L. specified the experimental 467 conditions and contributed to CO<sub>2</sub> data analysis and interpretation. J.P. conceptualized 468 dissolved carbon turnover in this study, and contributed to data interpretation and 469





470 paper writing. J.C. and J.Z. and X.W. provided comments on the manuscript. All authors reviewed and contributed to the final manuscript. 471 Acknowledgments 472 473 This study was financially supported by the National Natural Science Foundation of 474 China (NSFC grant no. U2244216, 42167050, 42407094), National Special Support Plan for High-Level Talent to Junbing Pu (Young Talent Plan, 2022), Natural Science 475 Foundation of Chongqing, China (CSTB2022NSCQ-LZX0022, 476 2024NSCQ-MSX3061), Guizhou Provincial Platform and Talent Program (YQK 477 [2023]017), Guizhou Provincial Science and Technology Projects (ZK[2024]061), 478 Science and Technology Plan for High-Level Young Talent of Guizhou Education 479 480 Department ([2024]325) and the Second Tibetan Plateau Scientific Expedition and

Research Program (Sub-item: 2019QZKK0601-3).





#### 482 References

- 483 An, Y., Hou, Y., Wu, Q., Qing, L., and Li, L.: Chemical weathering and CO<sub>2</sub> consumption of a
- 484 high-erosion-rate karstic river: a case study of the Sanchahe River, southwest China, Chinese
- 485 Journal of Geochemistry, 34, 601-609, 2015.
- 486 Binet, S., Probst, J. L., Batiot, C., Seidel, J. L., Emblanch, C., Peyraube, N., Charlier, J. B.,
- 487 Bakalowicz, M., and Probst, A.: Global warming and acid atmospheric deposition impacts on
- 488 carbonate dissolution and CO<sub>2</sub> fluxes in French karst hydrosystems: Evidence from hydrochemical
- 489 monitoring in recent decades, Geochimica et Cosmochimica Acta, 270, 184-200, 2020.
- 490 Bogard, M. J., Kuhn, C. D., Johnston, S. E., Striegl, R. G., Holtgrieve, G. W., Dornblaser, M. M.,
- 491 Spencer, R. G. M., Wickland, K. P., and Butman, D. E.: Negligible cycling of terrestrial carbon in
- many lakes of the arid circumpolar landscape, Nature Geoscience, 12, 180-185, 2019.
- 493 Borges, A. V., Deirmendjian, L., Bouillon, S., Okello, W., Lambert, T., Roland, F. A. E.,
- 494 Razanamahandry, V. F., Voarintsoa, N. R. G., Darchambeau, F., Kimirei, I. A., Descy, J.-P., Allen,
- 495 G. H., and Morana, C.: Greenhouse gas emissions from African lakes are no longer a blind spot,
- 496 Science Advances, 8, eabi8716, 2022.
- 497 Cao, J.-h., Wu, X., Huang, F., Hu, B., Groves, C., Yang, H., and Zhang, C.-l.: Global significance
- 498 of the carbon cycle in the karst dynamic system: evidence from geological and ecological
- 499 processes, China Geology, 1, 17-27, 2018.
- 500 Chen, H., Ju, P., Zhu, Q., Xu, X., Wu, N., Gao, Y., Feng, X., Tian, J., Niu, S., Zhang, Y., Peng, C.,
- 501 and Wang, Y.: Carbon and nitrogen cycling on the Qinghai-Tibetan Plateau, Nature Reviews Earth
- 502 & Environment, 3, 701-716, 2022.
- 503 Chen, L., Tan, L., Zhao, M., Sinha, A., Wang, T., and Gao, Y.: Karst carbon sink processes and
- effects: A review, Quaternary International, 652, 63-73, 2023.
- 505 D'Ettorre, U. S., Liso, I. S., and Parise, M.: Desertification in karst areas: A review, Earth-Science
- 506 Reviews, 253, 104786, 2024.
- 507 Drake, T. W., Podgorski, D. C., Dinga, B., Chanton, J. P., Six, J., and Spencer, R. G. M.: Land-use
- 508 controls on carbon biogeochemistry in lowland streams of the Congo Basin, Global Change Biol,
- 509 26, 1374-1389, 2020.
- 510 Evans, C. D., Futter, M. N., Moldan, F., Valinia, S., Frogbrook, Z., and Kothawala, D. N.:
- 511 Variability in organic carbon reactivity across lake residence time and trophic gradients, Nature
- 512 Geoscience, 10, 832-835, 2017.
- 513 Guo, Y., Gu, S., Wu, K., Tanentzap, A. J., Yu, J., Liu, X., Li, Q., He, P., Qiu, D., Deng, Y., Wang, P.,
- 514 Wu, Z., and Zhou, Q.: Temperature-mediated microbial carbon utilization in China's lakes, Global
- 515 Change Biol, 29, 5044-5061, 2023.
- Harjung, A., Ejarque, E., Battin, T., Butturini, A., Sabater, F., Stadler, M., and Schelker, J.:
- 517 Experimental evidence reveals impact of drought periods on dissolved organic matter quality and
- ecosystem metabolism in subalpine streams, Limnology and Oceanography, 64, 46-60, 2019.
- 519 He, H., Liu, Z., Li, D., Liu, X., Han, Y., Sun, H., Zhao, M., Shao, M., Shi, L., Hao, P., and Lai, C.:
- 520 Effects of carbon limitation and carbon fertilization on karst lake-reservoir productivity, Water
- 521 Research, 261, 122036, 2024.
- 522 He, H., Wang, Y., Liu, Z., Bao, Q., Wei, Y., Chen, C., and Sun, H.: Lake metabolic processes and





- their effects on the carbonate weathering CO<sub>2</sub> sink: Insights from diel variations in the
- 524 hydrochemistry of a typical karst lake in SW China, Water Research, 222, 118907, 2022a.
- 525 He, Q., Xiao, Q., Fan, J., Zhao, H., Cao, M., Zhang, C., and Jiang, Y.: The impact of heterotrophic
- 526 bacteria on recalcitrant dissolved organic carbon formation in a typical karstic river, Sci Total
- 527 Environ, 815, 152576, 2022b.
- 528 Hu, A., Choi, M., Tanentzap, A. J., Liu, J., Jang, K.-S., Lennon, J. T., Liu, Y., Soininen, J., Lu, X.,
- 529 Zhang, Y., Shen, J., and Wang, J.: Ecological networks of dissolved organic matter and
- microorganisms under global change, Nat Commun, 13, 3600, 2022.
- 531 Hu, J., Kang, L., Li, Z., Feng, X., Liang, C., Wu, Z., Zhou, W., Liu, X., Yang, Y., and Chen, L.:
- 532 Photo-produced aromatic compounds stimulate microbial degradation of dissolved organic carbon
- in thermokarst lakes, Nat Commun, 14, 3681, 2023.
- 534 Kellerman, A. M., Dittmar, T., Kothawala, D. N., and Tranvik, L. J.: Chemodiversity of dissolved
- organic matter in lakes driven by climate and hydrology, Nat Commun, 5, 3804, 2014.
- 536 Leles, S. G. and Levine, N. M.: Mechanistic constraints on the trade-off between photosynthesis
- and respiration in response to warming, Science Advances, 9, eadh8043, 2023.
- 538 Li, X., Wang, J., Lin, J., Yin, W., Shi, Y. Y., Wang, L., Xiao, H. B., Zhong, Z. M., Jiang, H., and
- 539 Shi, Z. H.: Hysteresis analysis reveals dissolved carbon concentration discharge relationships
- during and between storm events, Water Research, 226, 119220, 2022a.
- 541 Li, Y., Zhou, Y., Zhou, L., Zhang, Y., Xu, H., Jang, K.-S., Kothawala, D. N., Spencer, R. G. M.,
- 542 Jeppesen, E., Brookes, J. D., Davidson, T. A., and Wu, F.: Changes in Water Chemistry Associated
- 543 with Rainstorm Events Increase Carbon Emissions from the Inflowing River Mouth of a Major
- Drinking Water Reservoir, Environ Sci Technol, 56, 16494-16505, 2022b.
- Li, Y., Zhu, D., Niu, L., Zhang, W., Wang, L., Zhang, H., Zou, S., and Zhou, C.: Carbon-fixing
- 546 bacteria in diverse groundwaters of karst area: Distribution patterns, ecological interactions, and
- 547 driving factors, Water Research, 261, 121979, 2024.
- 548 Lindström, E. S. and Bergström, A.-K.: Influence of inlet bacteria on bacterioplankton assemblage
- 549 composition in lakes of different hydraulic retention time, Limnology and Oceanography, 49,
- 550 125-136, 2004.
- 551 Liu, S., Butman, D. E., and Raymond, P. A.: Evaluating CO<sub>2</sub> calculation error from organic
- alkalinity and pH measurement error in low ionic strength freshwaters, Limnology and
- 553 Oceanography: Methods, 18, 606-622, 2020.
- Liu, Z., Dreybrodt, W., and Wang, H.: A new direction in effective accounting for the atmospheric
- 555 CO<sub>2</sub> budget: Considering the combined action of carbonate dissolution, the global water cycle and
- 556 photosynthetic uptake of DIC by aquatic organisms, Earth-Science Reviews, 99, 162-172, 2010.
- 557 Liu, Z., Macpherson, G. L., Groves, C., Martin, J. B., Yuan, D., and Zeng, S.: Large and active
- 558 CO<sub>2</sub> uptake by coupled carbonate weathering, Earth-Science Reviews, 182, 42-49, 2018.
- Maberly, S. C., Barker, P. A., Stott, A. W., and De Ville, M. M.: Catchment productivity controls
- 560 CO<sub>2</sub> emissions from lakes, Nature Climate Change, 3, 391-394, 2013.
- 561 Mendonça, R., Müller, R. A., Clow, D., Verpoorter, C., Raymond, P., Tranvik, L. J., and Sobek, S.:
- Organic carbon burial in global lakes and reservoirs, Nat Commun, 8, 1694, 2017.
- 563 Monteith, D. T., Henrys, P. A., Hruška, J., de Wit, H. A., Krám, P., Moldan, F., Posch, M., Räike,
- 564 A., Stoddard, J. L., Shilland, E. M., Pereira, M. G., and Evans, C. D.: Long-term rise in riverine
- 565 dissolved organic carbon concentration is predicted by electrolyte solubility theory, Science
- 566 Advances, 9, eade3491, 2023.





- 567 Mu, C., Mu, M., Wu, X., Jia, L., Fan, C., Peng, X., Ping, C.-L., Wu, Q., Xiao, C., and Liu, J.: High
- 568 carbon emissions from thermokarst lakes and their determinants in the Tibet Plateau, Global
- 569 Change Biol, 29, 2732-2745, 2023.
- 570 Ni, M., Liu, R., Luo, W., Pu, J., Wu, S., Wang, Z., Zhang, J., Wang, X., and Ma, Y.: A
- 571 comprehensive conceptual framework for signaling in-lake CO<sub>2</sub> through dissolved organic matter,
- 572 Water Research, 264, 122228, 2024.
- Ni, M., Liu, R., Luo, W., Pu, J., Zhang, J., and Wang, X.: Unexpected shifts of dissolved carbon
- 574 biogeochemistry caused by anthropogenic disturbances in karst rivers, Water Research, 247,
- 575 120744, 2023.
- Ni, M., Ma, Y., Wang, Z., Wang, X., and Zhu, S.: A distinctive mode of dissolved organic carbon
- 577 biodegradation in karst lakes and reservoirs: Evidence from trophic controls and compositional
- 578 transformations, Journal of Cleaner Production, 368, 133217, 2022.
- 579 Ni, M. F., Li, S. Y., Luo, J. C., and Lu, X. X.: CO<sub>2</sub> partial pressure and CO<sub>2</sub> degassing in the
- Daning River of the upper Yangtze River, China, J Hydrol, 569, 483-494, 2019.
- 581 Ohno, T.: Fluorescence Inner-Filtering Correction for Determining the Humification Index of
- Dissolved Organic Matter, Environ Sci Technol, 36, 742-746, 2002.
- 583 Pi, X., Luo, Q., Feng, L., Xu, Y., Tang, J., Liang, X., Ma, E., Cheng, R., Fensholt, R., Brandt, M.,
- 584 Cai, X., Gibson, L., Liu, J., Zheng, C., Li, W., and Bryan, B. A.: Mapping global lake dynamics
- reveals the emerging roles of small lakes, Nat Commun, 13, 5777, 2022.
- Raymond, P. A. and Hamilton, S. K.: Anthropogenic influences on riverine fluxes of dissolved
- inorganic carbon to the oceans, Limnology and Oceanography Letters, 3, 143-155, 2018.
- 588 Raymond, P. A., Hartmann, J., Lauerwald, R., Sobek, S., McDonald, C., Hoover, M., Butman, D.,
- 589 Striegl, R., Mayorga, E., Humborg, C., Kortelainen, P., Durr, H., Meybeck, M., Ciais, P., and Guth,
- 590 P.: Global carbon dioxide emissions from inland waters, Nature, 503, 355-359, 2013.
- Rehn, L., Sponseller, R. A., Laudon, H., and Wallin, M. B.: Long-term changes in dissolved
- 592 inorganic carbon across boreal streams caused by altered hydrology, Limnology and
- 593 Oceanography, 68, 409-423, 2023.
- 594 Rodríguez-Cardona, B. M., Houle, D., Couture, S., Lapierre, J.-F., and del Giorgio, P. A.:
- 595 Long-term trends in carbon and color signal uneven browning and terrestrialization of northern
- lakes, Communications Earth & Environment, 4, 338, 2023.
- 597 Serikova, S., Pokrovsky, O. S., Laudon, H., Krickov, I. V., Lim, A. G., Manasypov, R. M., and
- Karlsson, J.: High carbon emissions from thermokarst lakes of Western Siberia, Nat Commun, 10,
- 599 1552, 2019.
- 600 Shangguan, Q., Payn, R. A., Hall Jr, R. O., Young, F. L., Valett, H. M., and DeGrandpre, M. D.:
- 601 Divergent metabolism estimates from dissolved oxygen and inorganic carbon: Implications for
- river carbon cycling, Limnology and Oceanography, 69, 2211-2228, 2024.
- 603 Song, K., Wen, Z., Xu, Y., Yang, H., Lyu, L., Zhao, Y., Fang, C., Shang, Y., and Du, J.: Dissolved
- 604 carbon in a large variety of lakes across five limnetic regions in China, Journal of Hydrology, 563,
- 605 143-154, 2018.
- 606 Sun, H., Han, C., Liu, Z., Wei, Y., Ma, S., Bao, Q., Zhang, Y., and Yan, H.: Nutrient limitations on
- 607 primary productivity and phosphorus removal by biological carbon pumps in dammed karst rivers:
- Implications for eutrophication control, Journal of Hydrology, 607, 127480, 2022.
- 609 Sun, P. a., He, S., Yu, S., Pu, J., Yuan, Y., and Zhang, C.: Dynamics in riverine inorganic and
- organic carbon based on carbonate weathering coupled with aquatic photosynthesis in a karst





- catchment, Southwest China, Water Research, 189, 116658, 2021.
- 612 Tranvik, L. J., Downing, J. A., Cotner, J. B., Loiselle, S. A., Striegl, R. G., Ballatore, T. J., Dillon,
- 613 P., Finlay, K., Fortino, K., Knoll, L. B., Kortelainen, P., Kutser, T., Larsen, S. H. H., Laurion, I.,
- 614 Leech, D. M., McCallister, S. L., McKnight, D. M., Melack, J. M., Overholt, E. P., Porter, J. A.,
- 615 Prairie, Y. T., Renwick, W. H., Roland, F., Sherman, B., Schindler, D. W., Sobek, S., Tremblay, A.,
- 616 Vanni, M. J., Verschoor, A. M., von Wachenfeldt, E., and Weyhenmeyer, G. A.: Lakes and
- 617 reservoirs as regulators of carbon cycling and climate, Limnology and Oceanography, 54,
- 618 2298–2314, 2009.
- 619 Tye, A. M., Williamson, J. L., Jarvie, H. P., Dise, N. B., Lapworth, D. J., Monteith, D., Sanders, R.,
- 620 Mayor, D. J., Bowes, M. J., Bowes, M., Burden, A., Callaghan, N., Farr, G., Felgate, S. L., Gibb,
- 621 S., Gilbert, P. J., Hargreaves, G., Keenan, P., Kitidis, V., Jürgens, M. D., Martin, A., Mounteney, I.,
- 622 Nightingale, P. D., Gloria Pereira, M., Olszewska, J., Pickard, A., Rees, A. P., Spears, B.,
- 623 Stinchcombe, M., White, D., Williams, P., Worrall, F., and Evans, C. D.: Dissolved inorganic
- 624 carbon export from rivers of Great Britain: Spatial distribution and potential catchment-scale
- 625 controls, Journal of Hydrology, 615, 128677, 2022.
- 626 Wang, H., Zhang, Q.-w., Chen, G., Li, X., Wang, Q.-l., Gao, L., Wang, J., He, D., and Li, M.: The
- 627 loss of dissolved organic matter from biological soil crust at various successional stages under
- rainfall of different intensities: Insights into the changes of molecular components at different
- 629 rainfall stages, Water Research, 257, 121719, 2024.
- 630 Wang, W., Li, S.-L., Zhong, J., Slowinski, S., Li, S., Li, C., Su, J., Yi, Y., Dong, K., Xu, S., Van
- 631 Cappellen, P., and Liu, C.-Q.: Carbonate mineral dissolution and photosynthesis-induced
- 632 precipitation regulate inorganic carbon cycling along the karst river-reservoir continuum, SW
- 633 China, Journal of Hydrology, 615, 128621, 2022.
- Ki, N., Zhang, T., Zhao, W., Jia, Y., Fan, J., Li, R., Li, J., and Pu, J.: Metabolic processes drive
- spatio-temporal variations of carbon sink/source in a karst river, Environmental Research, 262,
- 636 119970, 2024.
- 637 Xia, F., Liu, Z., Zhao, M., Li, Q., Li, D., Cao, W., Zeng, C., Hu, Y., Chen, B., Bao, Q., Zhang, Y.,
- He, Q., Lai, C., He, X., Ma, Z., Han, Y., and He, H.: High stability of autochthonous dissolved
- organic matter in karst aquatic ecosystems: Evidence from fluorescence, Water Research, 220,
- 640 118723, 2022.
- Xu, H., Xiao, Q., Dai, Y., Chen, D., Zhang, C., Jiang, Y., and Xie, J.: Selected Bacteria Are Critical
- 642 for Karst River Carbon Sequestration via Integrating Multi-omics and Hydrochemistry Data,
- 643 Microbial Ecology, 86, 3043-3056, 2023.
- Ku, Y. Y., Pierrot, D., and Cai, W. J.: Ocean carbonate system computation for anoxic waters using
- an updated CO<sub>2</sub>SYS program, Mar Chem, 195, 90-93, 2017.
- 646 Yan, Z., Xin, Y., Zhong, X., Yi, Y., Li, P., Wang, Y., Zhou, Y., He, Y., He, C., Shi, Q., Xu, W., and
- 647 He, D.: Evolution of dissolved organic nitrogen chemistry during transportation to the marginal
- sea: Insights from nitrogen isotope and molecular composition analyses, Water Research, 249,
- 649 120942, 2024.
- 650 Yi, Y., Zhong, J., Bao, H., Mostofa, K. M. G., Xu, S., Xiao, H.-Y., and Li, S.-L.: The impacts of
- 651 reservoirs on the sources and transport of riverine organic carbon in the karst area: A multi-tracer
- 652 study, Water Research, 194, 116933, 2021.
- 653 Yuan, Y., Liang, X., Li, Q., Deng, J., Zou, J., Li, G., Chen, G., Qin, W., and Dai, H.: Response of a
- 654 source water quality through a heavy precipitation event: Nutrients, dissolved organic matter and

https://doi.org/10.5194/egusphere-2025-4284 Preprint. Discussion started: 24 November 2025 © Author(s) 2025. CC BY 4.0 License.





- their DBPs formation, Journal of Cleaner Production, 453, 142273, 2024.
- Zhang, W., Wang, W., Zhong, J., Chen, S., Yi, Y., Xu, X., Chen, S., and Li, S.-L.: Carbon
- 657 sequestration and decreased CO<sub>2</sub> emission caused by biological carbon pump effect: Insights from
- diel hydrochemical variations in subtropical karst reservoirs, Journal of Hydrology, 632, 130909,
- 659 2024.
- 660 Zhao, R., Huang, S., Pu, J., He, Q., Wang, H., and Jiang, X.: Effects of rainfall on the karst-related
- carbon cycle due to carbonate rock weathering induced by H2SO4 and/or HNO3, Journal of
- 662 Hydrology, 630, 130664, 2024.



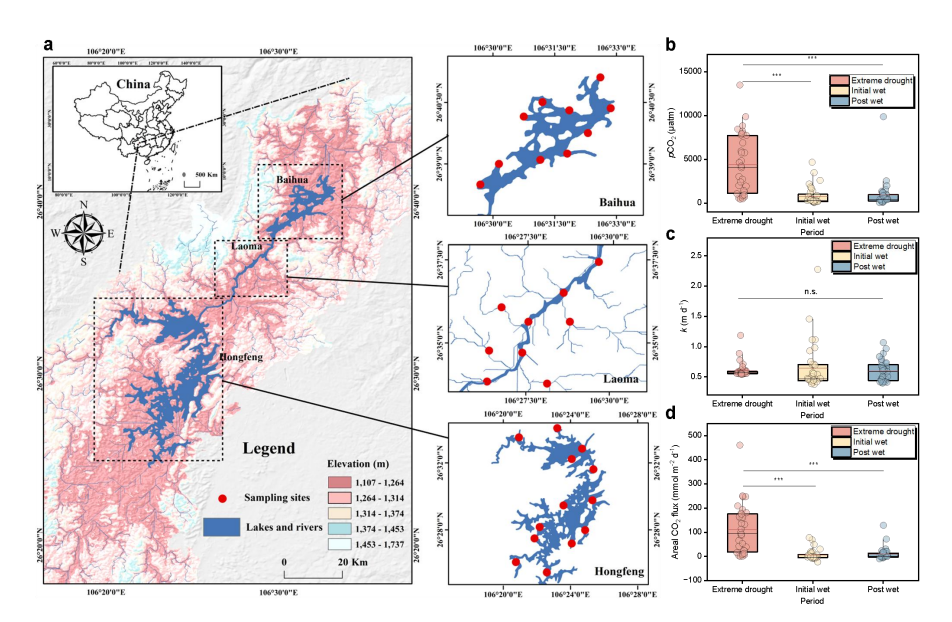


**Fig. 1.** Distribution of sampling locations and temporal patterns of CO<sub>2</sub> emissions in the karst lakes. (a) Map showing DEM information and observation sites. Variations of pCO<sub>2</sub> (b), k (c) and areal CO<sub>2</sub> flux (d) across extreme drought, initial wet and post wet periods. The boxes with bars represent 25%–75% percentiles with 5%–95% percentiles. Black lines, white lines and dots show median, mean and all data, respectively. Asterisks indicate statistical significance: \* p < 0.05, \*\* p < 0.01, \*\*\* p < 0.001.





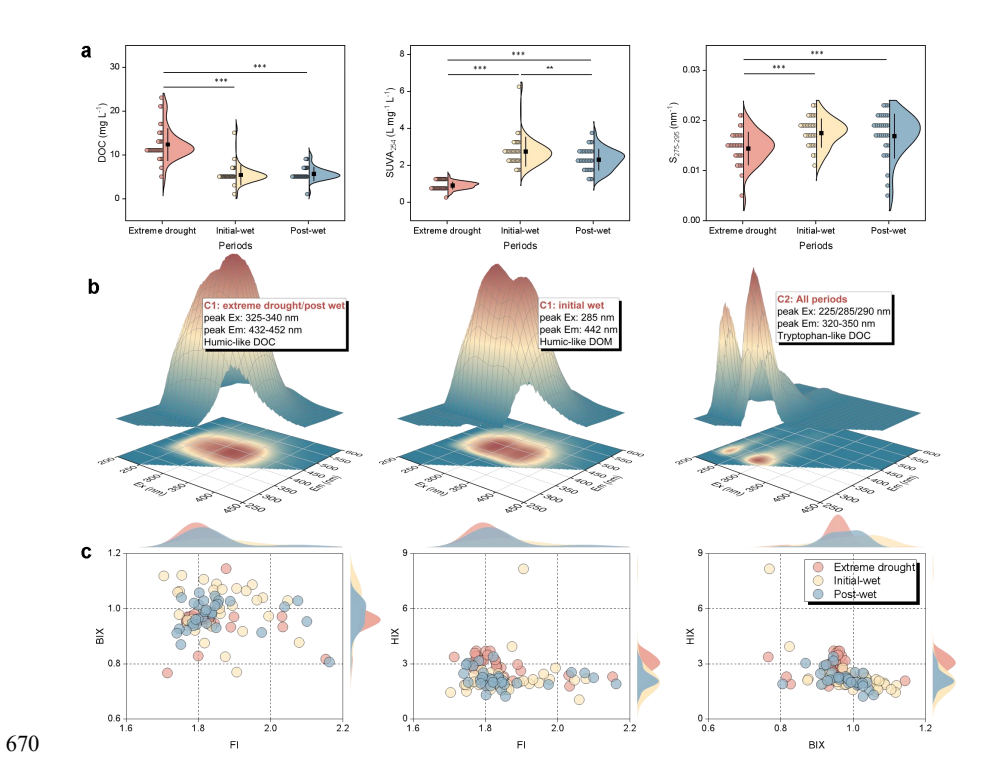


**Fig. 2.** Spectroscopic characteristics of DOC in the karst lakes. (a) Temporal patterns of DOC, SUVA<sub>254</sub> and S<sub>275-295</sub> over the study periods. Violins with dots represent Kernel Smooth distribution with all data. Black boxes with white bars show mean with standard deviation (s.d.). Asterisks indicate statistical significance: \*p < 0.05, \*\*p < 0.01, \*\*\* p < 0.001. (b) 3D view of primary DOC fluorophores identified by PARAFAC analysis. (c) Distributions of FI, BIX and HIX over the study periods. Dots correspond to all data of these fluorescent parameters. The waves show Kernel Smooth distributions of the data.





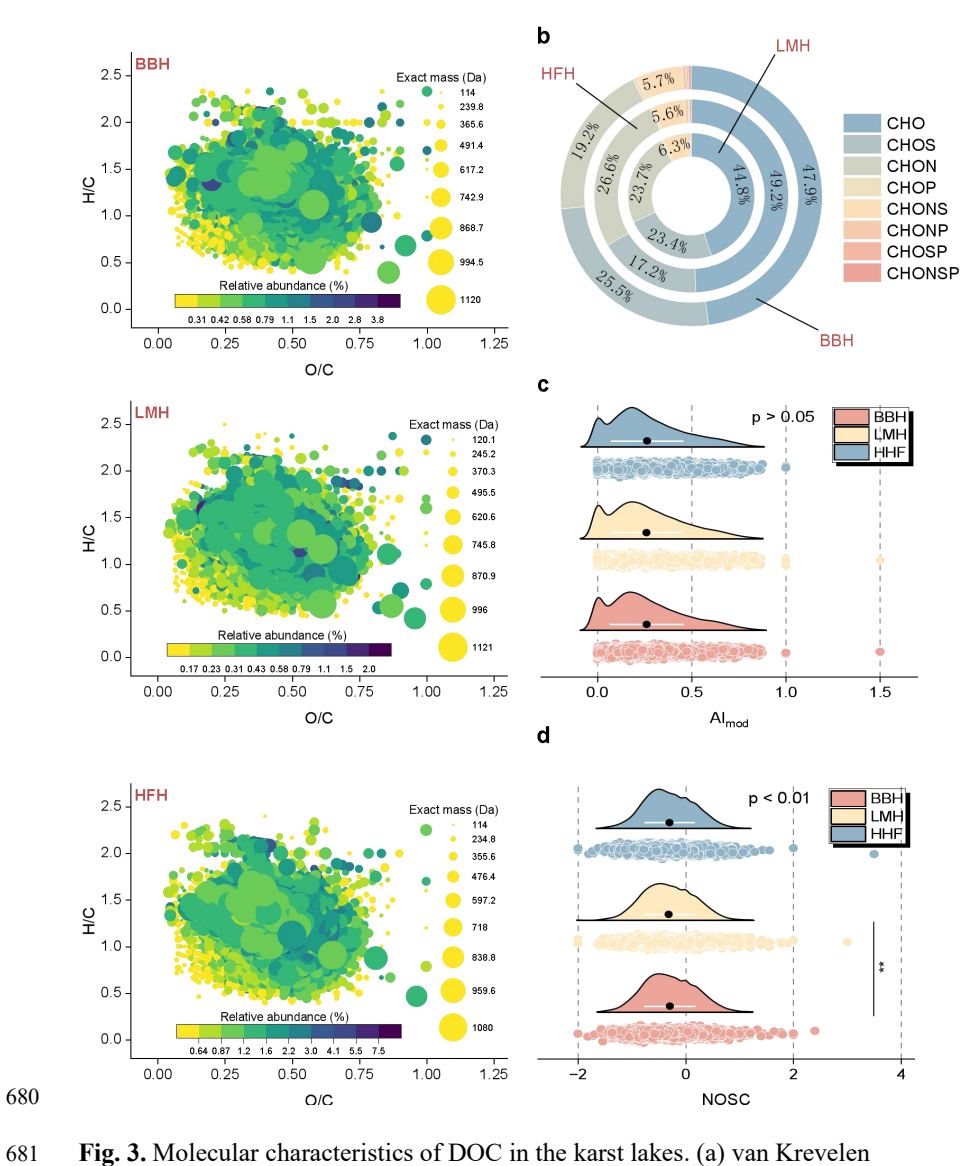


Fig. 3. Molecular characteristics of DOC in the karst lakes. (a) van Krevelen

Diagrams plotting H/C against O/C with exact mass information of DOC molecules. (b) Proportions of primary DOC molecular formulas across the lakes. The AI-mod (c) and NOSC (d) across lakes. Violins with dots represent Kernel Smooth distribution with all data. Black spots with white bars show mean with standard deviation (s.d.).

685 686

682

683





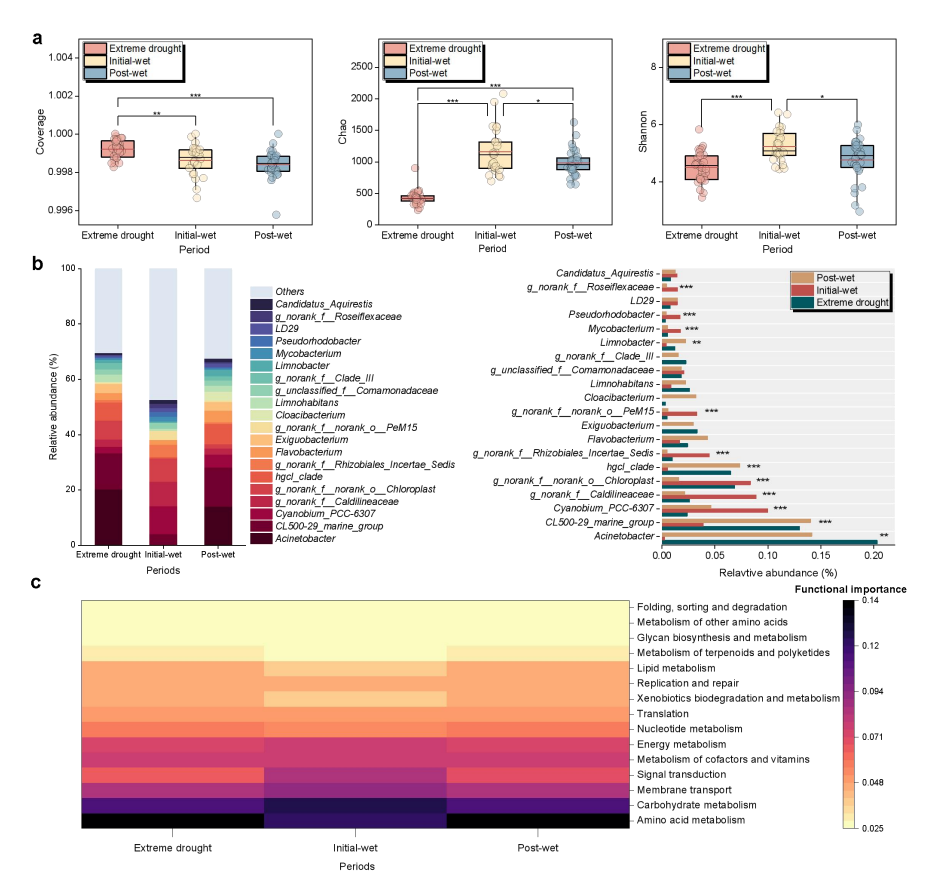


Fig. 4. Temporal variability of microbial communities and functions in the karst lakes.

(a) Alpha diversity indices regarding Coverage, Chao and Shannon over the study periods. The boxes with bars represent 25%–75% percentiles with 5%–95% percentiles. Black lines, white lines and dots show median, mean and all data, respectively. Asterisks indicate statistical significance: \* p < 0.05, \*\* p < 0.01, \*\*\* p < 0.001. (b) Comparison of the top 20 genera identified by relative abundance. (c) Potential microbial functions predicted by Tax4Fun based on the KEGG database.





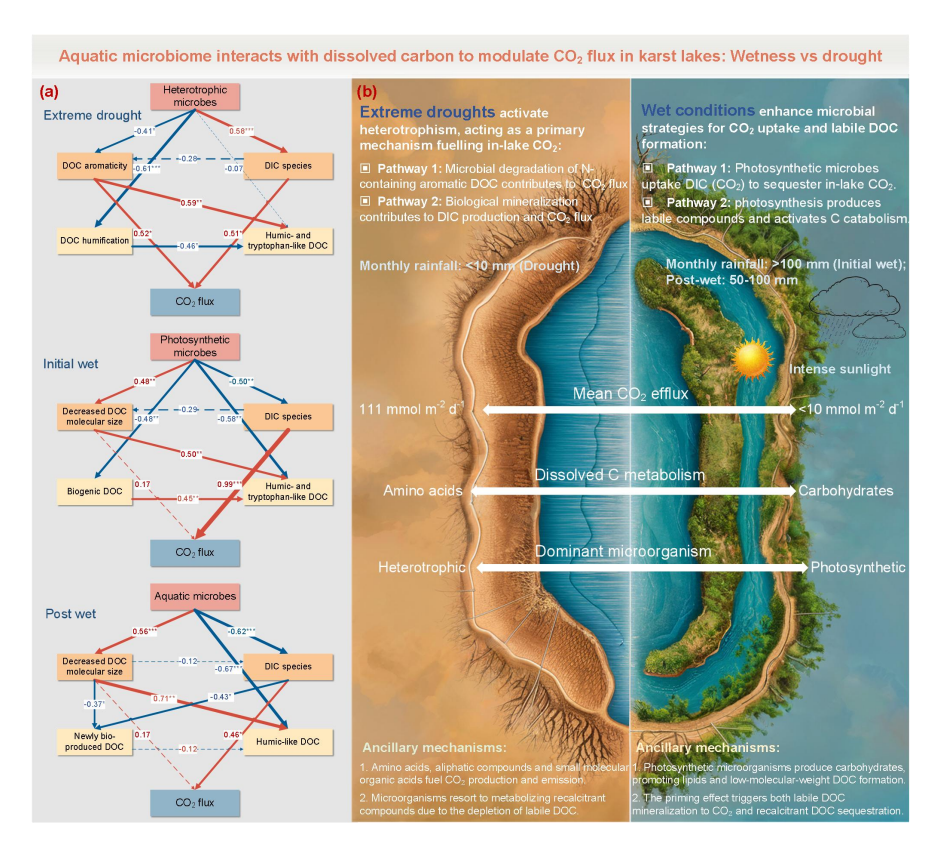


Fig. 5. Temporal pathways of aquatic microbiome-dissolved C interactions involved in CO<sub>2</sub> emission modulation in karst lakes. (a) The structural equation model showing temporal pathways of CO<sub>2</sub> flux driven by microbial communities and DIC-DOC turnover. Red and blue arrows represent positive and negative effects, respectively. Path coefficients are shown along the arrows. (b) A conceptual framework illustrating how microbiome interacts with dissolved carbon to modulate CO<sub>2</sub> emissions.





Table 1. Temporal patterns of pH, water temperature, total alkalinity and DIC speciesin the karst lakes.

	n	Min	Max	Median	Mean	Std. Dev
Extreme drought						
pН		6.71	8.30	7.20	7.40	0.48
Water temperature (°C)		14.5	19.5	16.2	16.2	0.99
Total alkalinity (µeq L-1)		2325.7	4940.9	2726.5	2960.5	703.2
DIC (µmol L-1)		2405.0	5272.5	2828.5	3114.2	668.8
HCO <sub>3</sub> - (µmol L-1)	32	2290.3	4895.5	2645.1	2878.6	655.0
$CO_3^{2-}$ (µmol L <sup>-1</sup> )	32	3.95	244.6	16.0	40.9	51.3
Dissolved CO <sub>2</sub> (µmol L <sup>-1</sup> )	32	18.0	602.4	177.0	194.7	153.5
Initial-wet						
pН	32	7.36	9.12	8.33	8.25	0.38
Water temperature (°C)	32	23.9	31.0	26.6	26.9	1.75
Total alkalinity (µeq L-1)	32	2178.7	6210.8	2895.3	3235.3	978.4
DIC (µmol L-1)	32	1538.7	6206.0	2688.8	3014.9	1042.5
HCO <sub>3</sub> - (µmol L-1)	32	918.4	5970.6	2428.0	2745.2	1073.0
CO <sub>3</sub> <sup>2-</sup> (µmol L <sup>-1</sup> )	32	35.7	752.7	218.2	243.5	155.1
Dissolved CO <sub>2</sub> (µmol L <sup>-1</sup> )	32	0.58	160.3	10.4	26.2	36.0
Post-wet						
pН	32	6.80	9.15	8.22	8.18	0.47
Water temperature (°C)	32	12.9	29.5	27.1	25.8	3.45
Total alkalinity (µeq L-1)	32	2239.7	5435.0	2795.5	3133.6	862.9
DIC (μmol L <sup>-1</sup> )		2096.8	5180.7	2576.5	2908.9	777.2
HCO <sub>3</sub> - (µmol L <sup>-1</sup> )		1546.7	4863.6	2441.5	2623.8	758.1
$CO_3^{2-}$ (µmol L <sup>-1</sup> )		6.27	887.9	195.5	253.5	222.5
Dissolved CO <sub>2</sub> (µmol L <sup>-1</sup> )		1.04	315.9	14.3	31.6	57.1